A comparison of multisensor attitude estimation algorithms

Chapter · September 2016

CITATIONS
6

READS
10,240

5 authors, including:

Pasquale Cirillo
Università degli Studi della Campania "Luigi Vanvitelli
18 PUBLICATIONS **230** CITATIONS
SEE PROFILE

Andrea Cirillo
Bitron Industrie S.p.A.
28 PUBLICATIONS **443** CITATIONS
SEE PROFILE

G. De Maria
Università degli Studi della Campania "Luigi Vanvitelli
146 PUBLICATIONS **2,001** CITATIONS
SEE PROFILE

Ciro Natale
Università degli Studi della Campania "Luigi Vanvitelli"
179 PUBLICATIONS **3,177** CITATIONS
SEE PROFILE

A. Cirillo, P. Cirillo, G. De Maria, C. Natale, S. Pirozzi

A comparison of multisensor attitude estimation algorithms

Contents

List of Figures

1

A comparison of multisensor attitude estimation algorithms

CONTENTS

1.1 Introduction

The accurate estimation of the orientation of a rigid body, relative to an inertial frame, is required for a wide range of applications. The recent development of low-cost and light-weight Micro Electro Mechanical Systems (MEMS) allowed the design of small and cheap Inertial Measurement Units (IMUs). They have had a successful impact both in several research areas and in consumer electronics. Widespread daily-life applications are mainly human-machine interfaces in smartphones and game consoles. Typical applications where inertial sensors are exploited in the professional service are real-time motion capture systems to track the location and the body posture of people [21, 27], gait analysis for rehabilitation purposes and biomedical applications as well as for performance assessment of the aging population [3, 26]. The use of inertial sensor-based systems is growing even in advanced robotic applications, e.g., localization and wheel slip estimation of a skid steered mobile robot [10], position and attitude determination for Micro Aerial Vehicles (MAVs) [24],

Unmanned Airborne Vehicles (UAVs) [11, 20] and Unmanned Underwater Vehicles (UUVs) [12].

1.1.1 The inertial measurement unit

An IMU provides real-time measurements of a tri-axial gyroscope and a tri-axial accelerometer, which can be employed for estimation of the orientation of a rigid body the IMU is attached to. These devices are based on MEMS technology and the *gyroscope* has some form of oscillating mass that, when the device changes orientation, is subject to a Coriolis force, orthogonal to the vibration direction and balanced by the elastic force causing the vibration itself. By measuring such force through a tri-axial capacitive displacement sensor, it is possible to indirectly measure the three components of the angular velocity during the rotation. The *accelerometer* observes the IMU's proper acceleration by measuring the weight experienced by a test mass elastically suspended again through a capacitive displacement sensor. When the accelerometer is placed in a gravitational field, and is not subjected to external non-gravitational accelerations, it measures the elastic force balancing the weight, and thus, it provides both the magnitude and direction of the gravitational acceleration.

The signal output of low-cost IMU systems, however, is characterized by low-resolution signals subject to high noise levels as well as general time-varying bias terms. Therefore, raw signals must be processed to reconstruct smoothed attitude estimates and bias-corrected angular velocity measurements through suitable sensor fusion algorithms. In fact, suitable exploitation of acceleration measurements can avoid drift caused by numerical integration of gyroscopic measurements. However, it is well-known that the use of only these two source of information cannot correct the drift of the estimated heading, thus an additional sensor is needed, i.e., a tri-axial *magnetometer*, which allows to obtain a correct heading estimation. In this case, the inertial unit is usually referred to as MARG (Magnetic Angular Rate and Gravity).

As said, in order to better estimate the orientation of a rigid body, angular velocity, linear acceleration and magnetic field data are fused together. Although many approaches have been adopted for filtering gyroscope data with inertial measurements, the most commonly used techniques are Extended Kalman filtering (EKF) and Complementary Filters. The methods based on the Kalman filter adopt a probabilistic determination of the state modeled as a Gaussian distribution given the system model [1, 2, 13]. The Complementary Filter is a valid alternative to the EKF-based methods given its simplicity and effectiveness. It uses a frequency domain analysis to filter the signals and combine them together to obtain an estimation of the orientation without any statistical description. Often, in robotic applications, e.g., UAVs, UUVs and MAVs control, the complementary filter is preferred to the EKF. This choice is justified by the higher computation time of the EKF-based algorithms due to its higher complexity. Most of the recent sensor fu-

sion algorithms for inertial/magnetic sensors provide orientation estimation in quaternion[1] form [16, 23]. Many other non linear estimation methods have been presented in the literature and the two proposed in [15] and [14] have attracted great interest in the robotics community. In particular, [15] formulate the filtering problem as a deterministic observer posed on the Special Orthogonal group $SO(3)$ termed 'explicit complementary filter'. In [14] the authors present a computationally efficient orientation algorithm based on optimized gradient descent algorithm designed to support a wearable inertial human motion tracking system for rehabilitation applications.

The contribution of this work is to carry out a comparison of the most popular attitude and heading estimation (AHRS) algorithms and an experimental validation using a robotic manipulator in order to define a reliable ground truth. In particular, the standard EKF framework and the methods proposed by [15] and by [14] have been considered worthy of particular interest. Although most of the papers in the literature propose modified versions of the EKF, e.g.[12], [7] and [25], the authors consider the standard EKF framework still a valid option. The main reasons are its generality and flexibility. In fact, this framework is particularly suitable to add and remove sensors without significantly changing the estimation algorithm, to take into account the different reliability and accuracy of sensors on the basis of their statistical characteristics, and to easily exploit all the a priori knowledge on the involved signals.

1.2 Sensor modeling and out-factory calibration

Low-cost sensors have much lower performance characteristics than high-end sensors for sophisticated applications. Therefore, an accurate calibration of such sensors is very important for the compensation of their systematic errors, i.e., bias and scale factors. Usually, accurate values of such parameters are not available from the manufacturer or they depend on the actual mounting of the MEMS components, which limits the use of these sensors for those applications that require high accuracy, such as human-machine interfaces, biomedical research and aerial robotics. To obtain a satisfactory performance, it is necessary to use a proper calibration method that could be performed in the background (self-calibration) or off-line by the system.

Three-axis accelerometers and three-axis magnetometers supplied for the consumer market are typically calibrated by the sensor manufacturer using a six-element linear model comprising a gain and offset in each of the three axes. This factory calibration can change as a result of the thermal stresses during

[1] Quaternions are a useful mathematical tool that require less computation time because of their minimal number of parameters and do not result in singularity configurations as the Euler representation does.

soldering of the accelerometer/magnetometer to the circuit board. Additional small errors, including rotation of the IC package relative to the circuit board and misalignment of the circuit board to the final product, can be introduced during the soldering and final assembly process. The original factory calibration will still be adequate for the vast majority of applications, however for professional applications this is not the case. In addition, the magnetometer behaviour can be influenced by the presence of hard-iron and soft-iron distortions that cannot be foreseen by the manufactures but are strictly related to the application. Hard-iron interference is normally generated by ferromagnetic materials with permanent magnetic fields that are part of the hand-held device structure. These materials could be permanent magnets or magnetized iron or steel. They are time invariant and their effect is to bias the magnetic sensor outputs. A soft-iron interference magnetic field is generated by the items inside the hand-held device. They could be the electric traces on the PCB or other magnetically soft materials.

1.2.1 Accelerometer/Magnetometer calibration

Calibration of accelerometers and magnetometers can be reduced to 3D-ellipsoid fitting problems [9], [5]. In the proposed calibration algorithm a six-parameter error model has been considered [19]. Denoting with $\boldsymbol{y}_f = [y_{f1}\ y_{f2}\ y_{f3}]^T$ a generic sensor output, a re-calibration procedure can be applied to compute the same six calibration parameters as the original factory calibration (a scale factor and an offset for each channel) but then applied on top of the factory calibrated output $\boldsymbol{y}_f$. The 3D fitting problem requires a set of measurements that should cover as much as possible the 3D space and, for the accelerometer calibration, it is necessary to carry out the measurements in a quasi-static condition to avoid accelerations other than the gravity. The re-calibrated sensor output $\hat{\boldsymbol{y}}^s$, expressed in the sensor frame Σ_s, become

$$\hat{\boldsymbol{y}}^s = \boldsymbol{\Lambda}\left(\boldsymbol{y}_f^s - \boldsymbol{b}^s\right) = \boldsymbol{\Lambda}\boldsymbol{y}_f^s - \boldsymbol{\Lambda}\boldsymbol{b}^s \tag{1.1}$$

where $\boldsymbol{\Lambda} = \mathrm{diag}\{\lambda_1, \lambda_2, \lambda_3\} > 0$ and $\boldsymbol{b}^s = [b_1\ b_2\ b_3]^T$ are the scale factors and offsets, respectively.

Objective of the calibration is to compute $\boldsymbol{\Lambda}$ and $\boldsymbol{b}$ such that the ellipsoid becomes a unit sphere centered in the origin, i.e.,

$$1 = \hat{\boldsymbol{y}}^{s^T}\hat{\boldsymbol{y}}^s = \boldsymbol{y}_f^{s^T}\boldsymbol{\Lambda}^2\boldsymbol{y}_f^s + \boldsymbol{b}^{sT}\boldsymbol{\Lambda}^2\boldsymbol{b}^s - 2\boldsymbol{y}_f^{s^T}\boldsymbol{\Lambda}^2\boldsymbol{b}^s \tag{1.2}$$

By introducing the following intermediate variables[2]

$$d = 1 - \boldsymbol{b}^{sT}\boldsymbol{\Lambda}^2\boldsymbol{b}^s \tag{1.3}$$

$$\bar{\boldsymbol{\Lambda}} = (1/d)\boldsymbol{\Lambda}^2 = \mathrm{diag}\{\bar{\lambda}_1, \bar{\lambda}_2, \bar{\lambda}_3\} \tag{1.4}$$

$$\boldsymbol{c} = (1/d)\boldsymbol{\Lambda}^2\boldsymbol{b}^s = \bar{\boldsymbol{\Lambda}}\boldsymbol{b}^s, \tag{1.5}$$

[2]Note that $d = 0$ can always be avoided by artificially translating the data.

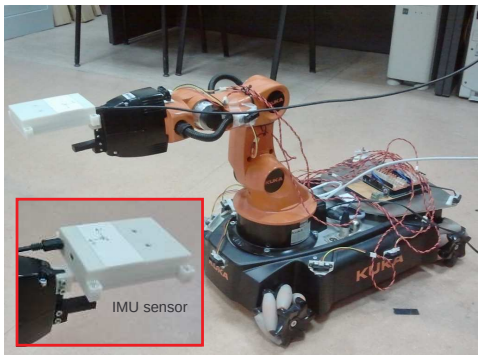

FIGURE 1.1
Experimental setup.

Eq. (1.2) can be written as

$$1 = \begin{bmatrix} y_{f1}^2 & y_{f2}^2 & y_{f3}^2 - 2y_{f1} - 2y_{f2} - 2y_{f3} \end{bmatrix} \begin{bmatrix} \bar{\lambda}_1 \\ \bar{\lambda}_2 \\ \bar{\lambda}_3 \\ \boldsymbol{c} \end{bmatrix}, \tag{1.6}$$

which can be easily solved by writing it for the entire measurement set as a linear system, by using a least square algorithm. The bias term $\boldsymbol{b}^s$ can be immediately computed from (1.5), while $\boldsymbol{\Lambda}^2$ can be computed by solving the linear system obtained substituting Eq. (1.3) into (1.4).

1.3 Experimental setup

The experimental setup is constituted by a KUKA robot and by a STM32F3Discovery board. The evaluation board is based on the STM32F303VCT6 ARM-Cortex M4 microcontroller, a ST L3GD20 3-axis digital output gyroscope, a ST LSM303DLHC MEMS system-in-package featuring a 3D digital linear acceleration sensor and a 3D digital magnetic sensor. In order to mechanically align the sensor frame to the robot end-effector frame and in order to avoid undesired rotations, the evaluation board is fixed to the robot gripper using a calibrated mechanical part. Figure 1.1 shows the experimental setup.

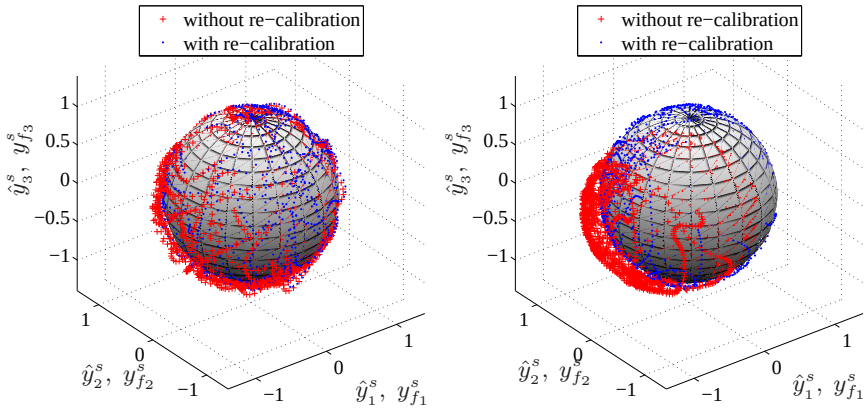

FIGURE 1.2
Calibration error of the accelerometer (left) and magnetometer (right) before and after re-calibration.

1.3.1 IMU

The considered IMU is constituted by ST MEMS motion sensors directly mounted on the STM32F3Discovery evaluation board. The ST L3GD20 3-axis gyroscope offers an I2C/SPI digital output interface, 16 bit value data output and three selectable ranges (±250, ±500, ±2000 dps) while the ST LSM303DLHC offers a 3-axis magnetometer with a full-scale from ±1.3 to ±8.1 Gauss and a 3-axis accelerometer with ±2 g/±4 g/±8 g/±16 g selectable range, 16 bit data output and a I2C serial interface. The experiments have been carried out by setting an acquisition rate of 760 Hz, 1344 Hz, 220 Hz and a full-scale range of ±2000 dps, ±2 g, ±1.3 Gauss for the gyroscope, the accelerometer and the magnetometer, respectively.

In order to improve the estimation accuracy, the calibration algorithm presented in Section 1.2 has been applied to both the magnetometer and the accelerometer of the adopted IMU and the results are reported in Fig. 1.2, where it is evident how the re-calibration allows to obtain a more spherical distribution of the samples.. In fact, after the re-calibration the standard deviation of $\|\hat{\boldsymbol{y}}^s\|$ is 2.8% for the magnetometer and 3.1% for the accelerometer, compared to the standard deviations of $\|\tilde{\boldsymbol{y}}_f^s\| = \|\boldsymbol{y}_f^s\|/\bar{\boldsymbol{y}}_f^s$ that are 17.9% and 5.2%, respectively, being $\bar{\boldsymbol{y}}_f^s$ the mean value of $\boldsymbol{y}_f^s$.

1.3.2 Robot

The robot used to compute the ground truth for performing the comparison among the attitude estimation algorithms is a KUKA Youbot [4] constituted by a 5-dof serial manipulator mounted on an omnidirectional platform. In

order to obtain a reference attitude with a clear geometrical interpretation, the first phase of the planned trajectory consists of rotating the three joints with orthogonal axes of the robot individually, while, in the second phase the joints are moved in a coordinated fashion so as generate rotations about the roll, pitch and yaw axes contemporarily. The joint angle values are measured using the robot encoders with a sampling frequency of 40 Hz.

1.4 Attitude estimation algorithms

As explained in Section 1.1, in this work three attitude estimation algorithms have been compared, one based on a standard EKF formulation and two specifically designed to solve the problem. As opposed to what one would expect from a specifically designed solution compared to a more general approach, the performance of the EKF will be demonstrated better in some cases than the other two methods, at the price of a higher computational burden. Nevertheless, the generality of the approach keeps the "door open" to further improvements that could come from the adoption of additional sensor (for example pressure sensor or GPS) data without the need to completely re-design the estimation algorithm and especially re-tune the algorithm parameters, which are based on the statistic characteristics of each signal.

1.4.1 Extended Kalman filter

Differently from the Kalman-based approaches proposed in [17] and [22], where modifications to the standard Bayesian framework were introduced with different motivations, the AHRS algorithm considered in this chapter, proposed in [6], is based on a standard EKF method. However, the modification proposed by [17] lead to a solution where handling of noise statistics is less trivial than in the standard EKF formulation, in fact noise rejection is delegated to a Gauss-Newton iterative algorithm, which is claimed less computational demanding than the standard EKF, but without a convincing evidence. The modification proposed by [22] consists in introducing the gyroscopic measurement directly in the state update equation rather than in the measurement equation, which implies the assumption of low noise affecting the sensor so as to allow a linearization of the update function. Finally, the recent survey on nonlinear attitude estimation techniques [8] recognizes that EKF-based approaches are the most used for two main reasons, their proven reliability and the ease of incorporation of further measurement sources that can improve the quality of the estimate or even provide estimate of further quantities, e.g. altitude and vertical velocity using pressure sensors or GPS, like in [25]. Moreover, the statistical characterization of the sensors required in the EKF

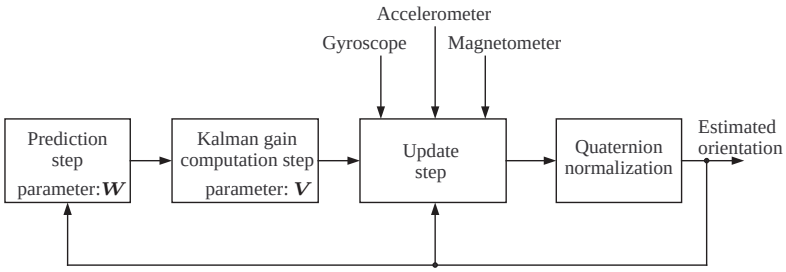

FIGURE 1.3
EKF algorithm block scheme.

framework allows tuning the algorithm parameters in a more straightforward fashion.

Figure 1.3 reports a block diagram of the considered EKF algorithm. Let Σ_v be the body-fixed frame. The augmented state considered in the EKF formulation is defined as

$$\boldsymbol{x}_k = \begin{bmatrix} \boldsymbol{Q}_k \\ \boldsymbol{\omega}_k^v \end{bmatrix}, \tag{1.7}$$

where $\boldsymbol{Q}_k$ is the quaternion expressing the estimated orientation and $\boldsymbol{\omega}_k^v$ is the angular velocity computed at the k-th step expressed in the body-fixed frame. Starting from the state vector computed at the k-th step, the orientation at the next step is computed through the Prediction step and the Kalman gain computation step using the knowledge on the process noise $\boldsymbol{W}$ and the measurement noise covariance matrix $\boldsymbol{V}$. Assuming the classical constant velocity model, the state update equation uses the gyroscope, accelerometer and magnetomer measurements to estimate the augmented state at the next step on the basis of the Kalman gain computed before. The quaternion normalization is used to prevent numerical issues due to the finite resolution of the numerical representation.

1.4.2 Madgwick's algorithm

Madgwick's algorithm is applicable to IMUs consisting of tri-axis gyroscopes and accelerometers sensor arrays that also include tri-axis magnetometers (MARG). The algorithm incorporates magnetic distortion compensation and it uses a quaternion representation, allowing accelerometer and magnetometer data to be used in an analytically derived and optimised gradient descent algorithm to compute the direction of the gyroscope measurement error as a quaternion derivative. Figure 1.4 reports a block diagram of the implemented filter, while, the equations of the algorithms can be found in [14]. The orientation of the rigid body is computed via two main processes. First, the gyroscope measurements are elaborated with a correction algorithm, which

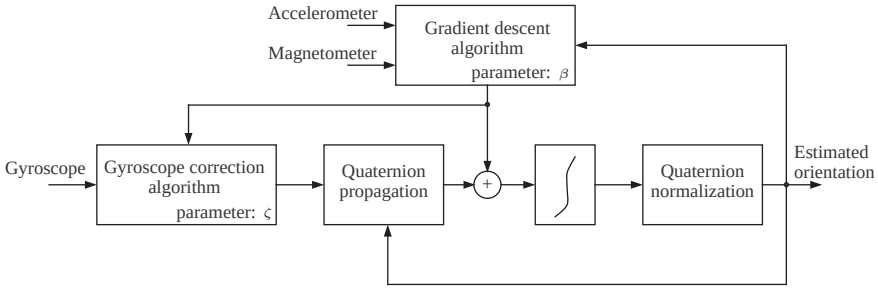

FIGURE 1.4
Madgwick's algorithm block diagram.

depends on the parameter ζ, in order to minimize the effects due to the bias and the drift error, and they are used to compute the body orientation with the quaternion propagation starting from the orientation estimated at the previous step. Then, accelerometer and magnetometer measurements are fused with a tunable parameter β through the gradient descent algorithm, which formulation is reported in [14]. The output of the gradient descent algorithm is then used to correct the orientation estimated by considering only gyroscope measurements.

1.4.3 Nonlinear complementary filter

In [15] authors propose the orientation estimation problem as a deterministic observation problem posed directly on the Special Orthogonal group $SO(3)$. Through the definition of a Direct Complementary Filter and a Passive Complementary Filter they arrive to a reformulation of the complementary filter, named Explicit Complementary Filter, in terms of direct vectorial measurements, such as gravitational or magnetic field directions obtained from an IMU. This observer does not require online algebraic reconstruction of attitude and is ideally suited for implementation on embedded hardware platforms owing to its low complexity. However, it suffers from possible discontinuities in the bias correction signal when the equivalent rotation angle of the estimated quaternion approaches $\pm\pi$ rad that could result in systematic errors in the reconstructed attitude. Fig.1.5 reports a block diagram of the algorithm. Starting from the knowledge of the body orientation computed at the previous step of the algorithm, an orientation error is obtained on the basis of the accelerometer and magnetometer measurements. A correction step based on a Proportional-Integral (PI) compensator is used to correct the measured angular velocity. Again, the quaternion propagation is integrated to obtain an estimate of the orientation, after the usual quaternion normalization.

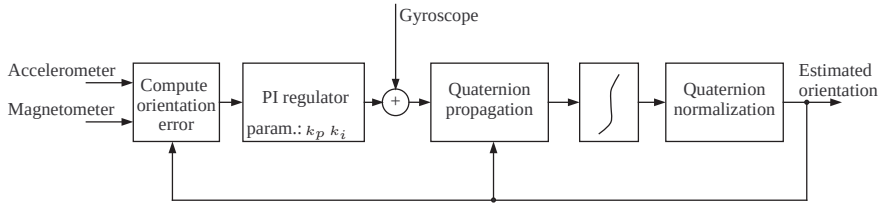

FIGURE 1.5
Mahony's algorithm block diagram.

1.5 Experimental results

The parameters of each of the three algorithms to be compared have been set as follows. For the EKF, the measurement covariance matrix $\boldsymbol{V}$ has been estimated by a simple static acquisition of the sensor signals and the resulting values are

$$\boldsymbol{V} = \text{diag}\{2.9 \cdot 10^{-5}, 2.3 \cdot 10^{-5}, 3.2 \cdot 10^{-5}, 3.1 \cdot 10^{-5}, \\ 4.5 \cdot 10^{-5}, 5.5 \cdot 10^{-5}, 2.0 \cdot 10^{-3}, 2.1 \cdot 10^{-3}, 2.0 \cdot 10^{-3}\}'$$

while the entries of the process covariance matrix have been tuned so as to obtain a satisfactory response time and a good noise rejection, as well as to guarantee filter convergence according to the result by [18], i.e.,

$$\boldsymbol{W} = \text{diag}\{10^{-10}, 10^{-10}, 10^{-10}, 10^{-10}, 10^{-3}, 10^{-3}, 10^{-3}\}.$$

Note how the first four entries are significantly lower than the others since the first four state equations in the EKF update step are the kinematic relation between angular velocity and time derivative of the quaternion, which is exact except for the numerical integration error.

The sole adjustable parameter of the algorithm recalled in Section 1.4.2 has been chosen as the optimal value proposed by [14] for the MARG implementation, i.e., $\beta = 0.041$ and $\zeta = 0.001$. The gain parameters of the algorithm recalled in Section 1.4.3 and implemented using the quaternion representation, have been chosen as proposed by [15], i.e., $k_p = 2$ and $k_i = 0.6$, which have been verified to be optimal also in this case.

The three algorithms have been implemented in Matlab/Simulink with a sampling time $T_s = 2\,\text{ms}$, since the sensor data have been acquired from the IMU at sampling frequency of 500 Hz, which is the frequency experimentally found to guarantee the most reliable communication. To compare the three AHRS algorithms, two robot trajectories are considered. In the first (slow) trajectory, an average speed of 18 deg/s is applied to robot joints, while, in the second (fast) trajectory, the average speed is raised to 45 deg/s. By defining

Σ_v the body-fixed frame and Σ_r the robot base frame, the ground truth is computed using the direct kinematics of the robot and, thus, computing the end-effector frame orientation (aligned to the body-fixed frame) in terms of the unit quaternion $\boldsymbol{Q}_{v,r}$. Let Σ_b be the base frame to which the orientation to be estimated is referred to. Thus, the estimated orientation of the body-fixed frame resulting from the AHRS algorithms $\hat{\boldsymbol{Q}}_{v,b}$, is compared with the ground truth $\boldsymbol{Q}_{v,b}$ (computed as $\boldsymbol{Q}_{v,b}(0) * \boldsymbol{Q}_{r,v}(0) * \boldsymbol{Q}_{v,r}(t)$) and the orientation error is calculated as the quaternion

$$\tilde{\boldsymbol{Q}}(t) = \hat{\boldsymbol{Q}}_{v,b}^{-1}(t) * \boldsymbol{Q}_{v,b}(t).$$

Figure 1.6 shows the estimated orientation, in quaternion representation, for both trajectories compared to the ground truth, where the reader can be observe the good performance of the three algorithms in terms of response time and noise rejection obtained with the parameters selected as explained above. The orientation error is then expressed in terms of Euler angles in Roll-Pitch-Yaw representation and it is reported in Fig. 1.7.

To quantify the algorithms performance, the standard deviation and the mean value are considered. The results of the experiments show that both in the slow and fast trajectories, the three algorithms provide comparable results in terms of accuracy.

TABLE 1.1
Mean and standard deviation of the attitude estimation error.

	EKF		Madgwick		Mahony	
Euler Angles [deg]	mean	std	mean	std	mean	std
Roll (slow)	-0.62	2.67	-0.61	2.75	-0.85	2.88
Pitch (slow)	-0.62	2.46	0.81	1.60	0.06	1.94
Yaw (slow)	-0.36	3.04	-1.01	2.23	-0.06	2.85
Roll (fast)	0.03	2.58	-0.33	2.12	-0.19	2.67
Pitch (fast)	-0.19	2.75	1.69	2.72	1.13	2.47
Yaw (fast)	-0.20	2.88	-2.11	2.94	-1.24	3.16

As a further analysis, a comparison on the computational burden of the considered algorithms has been carried out. In particular, the algorithms have been implemented in Matlab/Simulink environment on an Intel I7 quad-core processor at 1.6 GHz and they run at a sample rate of 2 ms. The tic-toc Matlab functions have been used to estimate the execution time of a single cycle that includes the gyroscope, accelerometer and magnetometer measurement and the attitude estimation. The flexibility of the EKF can be attributed to the availability of a tunable parameter for each sensor measurement, which is paid in terms of a higher execution time. Finally, to validate the proposed results, the algorithms have been coded for implementation on the STM32F3Discovery

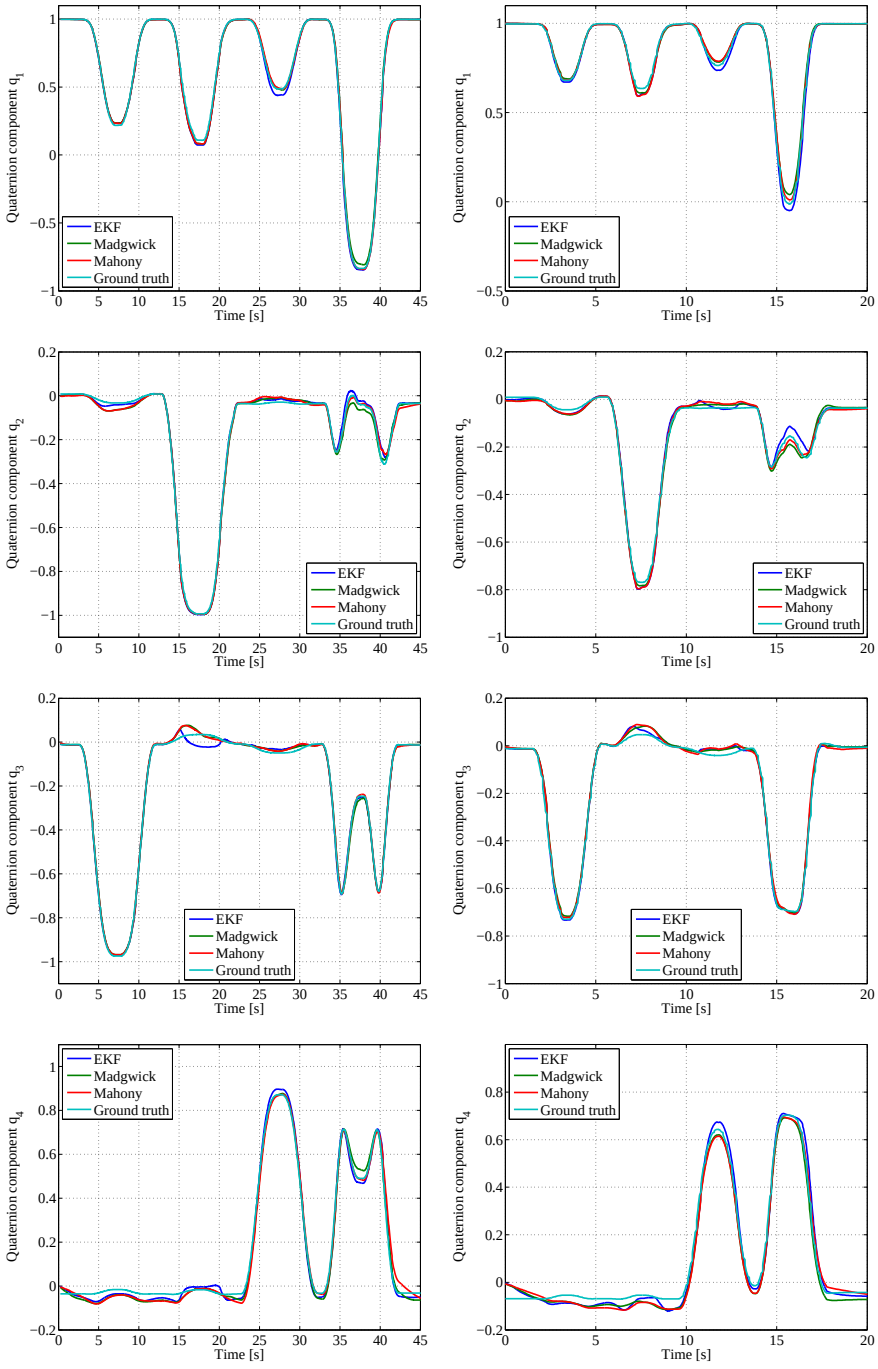

FIGURE 1.6
Estimated and true attitude and heading: slow trajectory (left) and fast trajectory (right).

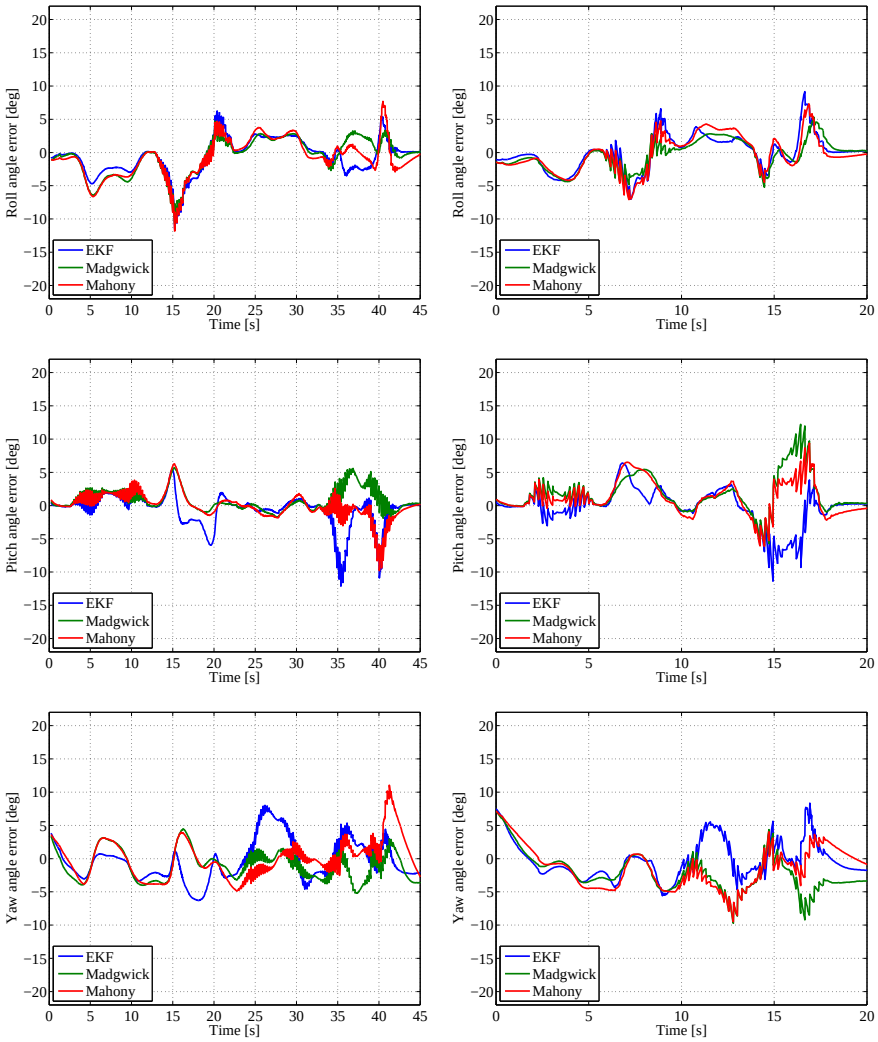

FIGURE 1.7
Orientation error: slow trajectory (left) and fast trajectory (right).

Algorithm	Matlab/Simulink [ms]	Embedded System [ms]
EKF	0.101	2.69
Madgwick	0.018	0.14
Mahony	0.013	0.12

TABLE 1.2
Computational burden estimation.

evaluation board using Chibi/OS as real-time embedded operating system. To this aim, the ARM Cortex Microcontroller Software Interface Standard (CMSIS) DSP library is used to implement the mathematical operations, i.e., matrix product and inverse. The sample rate is set to 3 ms for the EKF algorithm and to 2 ms for the Madgwick's and Mahony's algorithms. The Table 1.2 reports the average time required to compute one estimation cycle in both Matlab/Simulink environment and embedded system implementation, which refers to the maximum reachable frequency. Even though the execution times of the two fastest algorithms would allow to use a lower sampling time, this would lead to a negligible improvement due to the limited update rate of the magnetometer and gyroscope sensors.

1.6 Conclusions

In this chapter an experimental comparison of popular IMU-based algorithms for orientation estimation of a rigid body with respect to a reference frame is presented. In particular, two specifically designed solutions are compared to a standard EKF algorithm, which results to be similar in performance to the others, as experimentally demonstrated. However, its generality allows the user to add further sensory information, i.e., pressure sensing or GPS system, without the need to completely re-design the estimation filter or to re-tune the parameters of the algorithm, which are simply based on the statistics of the noise affecting each measured signal.

Bibliography

[1] *Generalized Multiplicative Extended Kalman Filter for Aided Attitude and Heading Reference System*, Toronto, Ontario Canada, 2010.

[2] A. Benini, Adriano Mancini, M. Marinelli, and Sauro Longhi. A biased extended kalman filter for indoor localization of a mobile agent using low-cost imu and uwb wireless sensor network. In *IFAC Proceedings Volumes (IFAC-PapersOnline)*, pages 735–740, 2012. cited By 0.

[3] C.L. Bennett, C. Odom, and M. Ben-Asher. Knee angle estimation based on imu data and artificial neural networks. In *Biomedical Engineering Conf. (SBEC)*, pages 111–112, 2013.

[4] R. Bischoff, U. Huggenberger, and E. Prassler. Kuka youbot - a mobile manipulator for research and education. In *IEEE Int. Conf. on Robotics and Automation (ICRA)*, pages 1–4, 2011.

[5] F. Camps, S. Harasse, and A. Monin. Numerical calibration for 3-axis accelerometers and magnetometers. In *IEEE Int. Conf. on Electro/Information Technology*, pages 217–221, 2009.

[6] A. Cavallo, A. Cirillo, P. Cirillo, G. De Maria, P. Falco, C. Natale, and S. Pirozzi. Experimental comparison of sensor fusion algorithms for attitude estimation. In *19th IFAC World Congress*, 2014.

[7] Shuai Chen, Cuiling Ding, Yu Han, Yunlei Fang, and Yanbing Chen. Study on information fusion algorithm for the miniature ahrs. In *4th Int. Conf. on Intelligent Human-Machine Systems and Cybernetics*, pages 114–117, 2012.

[8] John L. Crassidis, F. Landis Markley, and Yang Cheng. A survey of nonlinear attitude estimation methods. *J. of Guidance, Control, and Dynamics*, 30:12–28, 2007.

[9] Matthias Gietzelt, Klaus-Hendrik Wolf, Michael Marschollek, and Reinhold Haux. Performance comparison of accelerometer calibration algorithms based on 3d-ellipsoid fitting methods. *Computer Methods and Programs in Biomedicine*, 3:62–71, 2013.

[10] Yi Jingang, Zhang Junjie, Song Dezhen, and S. Jayasuriya. Imu-based localization and slip estimation for skid-steered mobile robots. In

IEEE/RSJ Int. Conf. on Intelligent Robots and Systems (IROS), pages 2845–2850, 2007.

[11] Han Joong-hee, J.H. Kwon, Lee Impyeong, and Choi Kyoungah. Position and attitude determination for uav-based gps, imu and at without gcps. In *Int. Workshop on Multi-Platform/Multi-Sensor Remote Sensing and Mapping (M2RSM)*, pages 1–5, 2011.

[12] Ho-Sung Kim, Hyeung-Sik Choi, Jong su Yoon, and P.I. Ro. Study on ahrs sensor for unmanned underwater vehicle. *Int. J. of Ocean System Engineering*, 1:165–170, 2011.

[13] Gabriele Ligorio and Angelo Maria Sabatini. Extended kalman filter-based methods for pose estimation using visual, inertial and magnetic sensors: Comparative analysis and performance evaluation. *Sensors*, 13(2):1919, 2013.

[14] S.O.H. Madgwick, A.J.L. Harrison, and R. Vaidyanathan. Estimation of imu and marg orientation using a gradient descent algorithm. In *IEEE Int. Conf. on Rehabilitation Robotics (ICORR)*, pages 1–7, 2011.

[15] R. Mahony, T. Hamel, and Jean-Michel Pflimlin. Nonlinear complementary filters on the special orthogonal group. *IEEE Trans. on Automatic Control*, 53:1203–1218, 2008.

[16] J.L. Marins, X. Yun, E.R. Bachmann, R.B. McGhee, and M.J. Zyda. An extended kalman filter for quaternion-based orientation estimation using marg sensors. In *Intelligent Robots and Systems, 2001. Proceedings. 2001 IEEE/RSJ International Conference on*, volume 4, pages 2003–2011 vol.4, 2001.

[17] J.L. Marins, X. Yun, E.R. Bachmann, R.B. McGhee, and M.J. Zyda. Extended kalman filter for quaternion-based orientation estimation using marg sensors. In *Proc. of the 2001 IEEE/RSJ Int. Conf. on Intelligent Robots and Systems*, pages 2003–2011, 2001.

[18] C. Natale. Kinematic control of robots with noisy guidance system. In *Proc. of the 18th IFAC World Congress*, pages 6937–6944, 2011.

[19] Mark Pedley. High precision calibration of a three-axis accelerometer - an4399. Technical report, Freescale Semiconductor, 2013.

[20] C. Perez-D'Arpino, D. Vigouroux, W. Medina-Melendez, L. Fermin, R.R. Torrealba, J.C. Grieco, and G. Fernandez-Lopez. Development of a low cost inertial measurement unit for uav applications with kalman filter based attitude determination. In *Technologies for Practical Robot Applications (TePRA), 2011 IEEE Conference on*, pages 178–183, April 2011.

[21] I. Prayudi and Kim Doik. Design and implementation of imu-based human arm motion capture system. In *Int. Conf. on Mechatronics and Automation (ICMA)*, pages 670–675, 2012.

[22] A.M. Sabatini. Quaternion-based extended kalman filter for determining orientation by inertial and magnetic sensing. *IEEE Trans. on Biomedical Engineering*, 53:1346–1356, 2006.

[23] Young Soo Suh. Orientation estimation using a quaternion-based indirect kalman filter with adaptive estimation of external acceleration. *Instrumentation and Measurement, IEEE Transactions on*, 59(12):3296–3305, Dec 2010.

[24] ClarkN. Taylor. Enabling navigation of mavs through inertial, vision, and air pressure sensor fusion. In Hernsoo Hahn, Hanseok Ko, and Sukhan Lee, editors, *Multisensor Fusion and Integration for Intelligent Systems*, volume 35 of *Lecture Notes in Electrical Engineering*, pages 143–158. Springer Berlin Heidelberg, 2009.

[25] L. Xia, J. Wang, and Y. Liu. Quadratic ekf algorithm enhancements for low cost tightly-coupled ahrs/gps. In *2nd Int. Symposium on Systems and Control in Aerospace and Astronautics*, pages 1–6, 2008.

[26] M. Zecca, K. Saito, S. Sessa, L. Bartolomeo, Z. Lin, S. Cosentino, H. Ishii, T. Ikai, and A. Takanishi. Use of an ultra-miniaturized imu-based motion capture system for objective evaluation and assessment of walking skills. In *35th Annual Int. Conf. of the IEEE Engineering in Medicine and Biology Society (EMBC)*, pages 4883–4886, 2013.

[27] J. Ziegler, H. Kretzschmar, C. Stachniss, G. Grisetti, and W. Burgard. Accurate human motion capture in large areas by combining imu- and laser-based people tracking. In *IEEE/RSJ Int. Conf. on Intelligent Robots and Systems (IROS)*, pages 86–91, 2011.